The Influence of Southern Ocean Winds on the North Atlantic Carbon Sink

Ben Bronselaer[1], Laure Zanna[1] David R. Munday[1,2], and Jason Lowe[3]

Corresponding author: B. Bronselaer, Atmospheric, Oceanic and Planetary Physics, Department of Physics, University of Oxford, Oxford, OX1 3PU, UK. (benjamin.bronselaer@physics.ox.ac.uk)

[1]Atmospheric, Oceanic and Planetary Physics, Department of Physics, University of Oxford, Oxford, OX1 3PU, UK.

[2]British Antarctic Survey, Madingley Road, Cambridge, CB3 0ET, UK

[3]Met Office Hadley Centre, FitzRoy Road, Exeter, Devon EX1 3PB, UK

This article has been accepted for publication and undergone full peer review but has not been through the copyediting, typesetting, pagination and proofreading process, which may lead to differences between this version and the Version of Record. Please cite this article as doi: 10.1002/2015GB005364

Abstract.

Observed and predicted increases in Southern Ocean winds are thought to upwell deep ocean carbon and increase atmospheric CO_2. However, Southern Ocean dynamics affect biogeochemistry and circulation pathways on a global scale. Using idealised MITgcm simulations, we demonstrate that an increase in Southern Ocean winds reduces the carbon sink in the North Atlantic sub-polar gyre. The increase in atmospheric CO_2 due to the reduction of the North Atlantic carbon sink is shown to be of the same magnitude as the increase in atmospheric CO_2 due to Southern Ocean outgassing. The mechanism can be described as follows: The increase in Southern Ocean winds leads to an increase in upper ocean northward nutrient transport. Biological productivity is therefore enhanced in the tropics, which alters the chemistry of the sub-thermocline waters that are ultimately upwelled in the sub-polar gyre. The results demonstrate the influence of Southern Ocean winds on the North Atlantic carbon sink and show that the effect of Southern Ocean winds on atmospheric CO_2 is likely twice as large as previously thought in past, present, and future climates.

Key points.

- Increased Southern Ocean winds reduce the North Atlantic carbon sink.
- The effect of Southern Ocean winds on atmospheric pCO_2 is doubled by the non-local feedback.
- Atlantic tropical biology affects the North Atlantic sub-polar gyre Revelle Buffer Factor.

1. Introduction

Paleo-proxy and historical data show large changes in atmospheric pCO_2, indicating variations in the atmosphere-ocean exchange of carbon. Changes in atmospheric forcing, such as Southern Hemisphere westerly wind stress, can have a strong influence on the carbon cycle. The impact of observed and projected Southern Ocean wind increase [*Swart et al.*, 2014; *Bracegirdle et al.*, 2013] on the Southern Ocean carbon flux has been extensively studied [e.g., *Le Quere et al.*, 2007; *Lovenduski et al.*, 2008; *Lovenduski and Ito*, 2009; *Ito et al.*, 2010; *Lauderdale et al.*, 2013; *Munday et al.*, 2014]. Increased Southern Ocean winds are thought to increase upwelling of deep ocean natural carbon, elevating local ocean pCO_2. The elevated ocean pCO_2 leads to a reduction in local sink of anthropogenic CO_2 and a subsequent increase in atmospheric CO_2 levels.

However, little attention has gone into estimating the climate impacts of dynamical and biogeochemical changes induced by the Southern Ocean wind stress outside of the Southern Ocean. The Southern Ocean circulation forms part of the global meridional overturning circulation [*Gnanadesikan*, 1999; *Marshall and Speer*, 2012] and has a strong influence on transport pathways [*Ito et al.*, 2010; *Palter et al.*, 2010], including in the North Atlantic. Southern Ocean winds act to ventilate the deep ocean, which is richer in nutrients than the surface ocean. The wind-driven ventilation in the Southern Ocean mixes nutrients into the surface ocean, giving it a large effect on ocean biogeochemistry and biological productivity on a global scale [*Marinov et al.*, 2006]. *Anderson et al.* [2002] and *Sarmiento et al.* [2004] show that increased Southern Ocean upwelling increases nutrient supply north of the Southern Ocean and enhances high- and low-latitude biological

productivity. Changes induced in the Southern Ocean can therefore have far-reaching impact on ocean dynamical and biogeochemical properties.

Studies such as *Lauderdale et al.* [2013] examine the basin-scale response to Southern Ocean wind stress perturbations on the dynamics and distribution of carbon, but focus on the local contribution of wind stress on atmospheric pCO_2. The non-local effect of the Southern Ocean winds on atmospheric CO_2, via change in global-scale transport pathways and in nutrient export from the Southern Ocean, remains to be estimated. We focus primarily on understanding the response of other major carbon sinks to changes induced in the Southern Ocean.

In the Atlantic, the major oceanic sink of atmospheric carbon (both natural and anthropogenic) is the sub-polar gyre [*Group*, 1998; *Dickson et al.*, 2008; *Khatiwala et al.*, 2009; *Kieke and Yashayaev*, 2014]. Any changes in the North Atlantic ocean carbon chemistry will therefore greatly impact the magnitude of the local carbon sink and subsequently alter atmospheric CO_2 levels. *Halloran et al.* [2015], for example, show that the biogeochemical properties of the sub-polar gyre are affected by the water advected from the Tropics and Southern Ocean. Southern Ocean winds have the potential to influence the North Atlantic carbon sink by affecting the biogeochemical properties of the waters advected from the Southern Ocean to the North Atlantic.

The aim of this paper is to assess the non-local effect of Southern Ocean winds on atmospheric CO_2 and to demonstrate that increased Southern Ocean winds affect the North Atlantic pCO_2 through a novel mechanism. The mechanism can be summarized as follows: increased Southern Ocean wind stress enhances nutrient transport towards the Tropics, thereby increasing tropical biological productivity. This in turn affects the

chemistry of underlying sub-thermocline waters. The tropical sub-thermocline waters are subsequently advected to the North Atlantic sub-polar gyre by equatorial currents and the meridional overturning circulation (MOC), reducing the capacity of the sub-polar gyre to absorb atmospheric CO_2.

The paper is structured as follows. We provide a description of the model used in this paper in section 2, with details regarding the model design and mean state. Section 3 describes and quantifies the effect of Southern Ocean wind perturbations on the North Atlantic carbon sink. The subsequent section 4 will the detail the key steps in the mechanism and section 5 summarizes the main conclusion, caveats and implications of the presented study.

2. Model design and control experiment

To study the effect of Southern Ocean winds on the North Atlantic carbon sink, we use the MIT General Circulation Model [MITgcm, *Marshall et al.*, 1997] in an idealised configuration designed to mimic the Atlantic and Southern Oceans. The set-up and parameters are similar to *Munday et al.* [2014] at 2°x2° horizontal grid spacing with eddies parametrized using the Gent-McWilliams [*Gent and McWilliams*, 1990] scheme with a constant coefficient. The domain, shown in Fig. 1A, is a sector 20°-wide in longitude, extending to 60°N/S with a re-entrant channel between 60° and 40°S to allow for a circumpolar current. The basin is 5000m deep, except at the channel boundaries where a 2500m deep sill represents Drake Passage. Coupled to the ocean, there is a well-mixed atmospheric box which only solves for atmospheric pCO_2 and the air-sea flux of carbon is parametrized following *Wanninkhof* [1992]. The model resolution is chosen such

that a large set of perturbation experiments can be run for centuries while still capturing the main features of a large-scale circulation and the appropriate response of the ocean carbon cycle. Such a setup is widely used to conduct large-scale ocean studies [e.g., *Wolfe and Cessi*, 2010; *Ito and Follows*, 2003; *Munday et al.*, 2013].

The model is forced with a zonal wind stress profile shown in Fig. 1B with $\overline{\tau_{SO}} = 0.13\text{N/m}^2$ (where the subscipt "SO" indicates the Southern Ocean between $60° - 40°$S and the overline indicates a spatial average). Heat and freshwater fluxes are prescribed through temperature and salinity restoring profiles (Figs.1C and 1D), which broadly match the observed distributions in the Atlantic. The resulting residual (sum of Eulerian and eddy) overturning streamfunction is shown in Fig. 1E [*Marshall and Radko*, 2003].

The model also supports a series of equatorial and mid-latitude zonal currents, with a westward equatorial current, an eastward undercurrent [*Knauss*, 1960; *Philander*, 1973; *Wyrtki and Kilonsky*, 1984; *Philander et al.*, 1987] and a series of stationary eastward jets on either side of the equator [*Tsuchiya*, 1972; *Firing et al.*, 1998; *Rowe et al.*, 2000; *Izumo et al.*, 2002; *Qiu et al.*, 2013] (Fig. 1F). While the structures are similar to observations, the magnitude of the currents in the MITgcm are smaller, likely due to the model geometry and its coarse horizontal and vertical resolution. The equatorial jets, alongside vertical and horizontal mixing, are important factors for ventilation of the shadow zone [*Brandt et al.*, 2015]: a region of the sub-surface ocean that is unventilated by the wind-driven gyre circulation.

The ocean model contains a biogeochemical component with 7 tracers: dissolved inorganic carbon (DIC), alkalinity, preformed alkalinity, phosphate, preformed phosphate, dissolved organic phosphorous, and dissolved oxygen [*Dutkiewicz et al.*, 2008; *Follows*

et al., 2006]. Biological productivity is governed by phosphate and light limitation. Figure 2A-C shows the zonally averaged distribution of DIC, regenerated DIC and dissolved oxygen. The maximum in DIC concentration is located in the abyssal cell at high latitudes where water is oldest. Regenerated DIC concentrations are generally high where dissolved oxygen concentrations are low since oxygen is used up in the remineralisation of soft organic matter. The upper ocean distributions of DIC and Alkalinity are in agreement in with GLODAP climatology [*Key et al.*, 2004].

The model shows the presence of an oxygen minimum zone (OMZ) in the shadow zone between 100-1000m depth, with corresponding high regenerated carbon concentrations. The lack of wind-driven ventilation in the shadow zone leads to a build up of organic carbon and the associated removal of dissolved oxygen. The meridional and vertical extent of the OMZ compares well with other studies such as *Ito and Follows* [2005] although the magnitude is slightly higher in the presented model compared to other studies. For a more detailed description of the distribution of biogeochemical tracers in the model, see *Munday et al.* [2014].

Mixed layer biological activity is shown in Fig. 3A, with higher activity at high latitudes than at the equator and little biological activity in the oligotrophic sub-tropical regions. Such patterns are supported by satellite chlorophyll observations and other models [*Williams and Follows*, 2011]. The efficiency of the biological pump in the model (given by the ratio of mixed layer nutrient concentration over the nutrient concentration at 100-200m depth), at high latitudes is 0.1-0.2 while in the tropics it is between 0.6 and 0.8. These numbers are consistent with observations [*Sarmiento et al.*, 2004]. The spatial pattern, including the large-scale meridional gradients of pCO_2, shown in Fig. 3B,

is comparable to observations [*Takahashi et al.*, 2009; *Valsala and Maksyutov*, 2010]. As a result, there is a positive air-sea flux of carbon north of the Southern channel and in the Northern sub-polar region ($40° - 60°$N), and a negative air-sea flux of carbon in the Southern channel and Tropics, again consistent with observations [*Takahashi et al.*, 2009] (Fig. 3C). Overall, the large-scale distribution and magnitude of the biogeochemical tracers agrees well with other studies [e.g., *Ito and Follows*, 2005] and observations [*Feely et al.*, 2001; *Gruber*, 1998].

3. The response of the North Atlantic carbon sink to increased Southern Ocean wind stress

3.1. The North Atlantic carbon flux

To examine the response of the carbon system to Southern Ocean wind stress perturbations, the wind stress between 60° and 20°S, τ_{SO}, is multiplied by a constant in a set of numerical experiments (see Fig. 1B). Each perturbed experiment is run for 400 years, after which time the dynamics of the upper 1000m has fully equilibrated. We will examine the carbon cycle response to a range of wind stress perturbations, while specific examples will be drawn from the $2 \times \tau_{SO}$ scenario. The $2 \times \tau_{SO}$ experiment was run for 3000 years to verify that the results are not dependent on the length of integration. The response of the circulation to changes in Southern Ocean wind is linear. The Ekman transport and strength of the upper overturning cell increase linearly with wind stress. Our results therefore scale with forcing scenarios without non-linear behaviour.

Figure 4 illustrates the impact of ocean $p\mathrm{CO}_2$, $p\mathrm{CO}_2^o$, in the North Atlantic sub-polar gyre on atmospheric $p\mathrm{CO}_2$, $p\mathrm{CO}_2^a$. Fig. 4 shows time series of atmospheric $p\mathrm{CO}_2$ (panel A), the area-averaged ocean $p\mathrm{CO}_2$ for the North Atlantic sub-polar gyre ($40° - 60°$N, panel

B) and the Southern Ocean ($40° - 60°$S, panel C) in the $2 \times \tau_{SO}$ wind stress perturbation experiment. The initial adjustment of the Southern Ocean $p\mathrm{CO}_2^o$ occurs within the first few decades. The atmospheric $p\mathrm{CO}_2$ shows an initial increase over a few decades which coincides with the timescale of the local response of the Southern Ocean $p\mathrm{CO}_2^o$. However, the short-term response is followed by a long-term centennial adjustment in pCO_2^a due to the perturbed ocean carbon reservoir in the North Atlantic. We refer to the atmospheric $p\mathrm{CO}_2^a$ anomalies induced by the North Atlantic sub-polar gyre as the non-local effect, with a timescale set by the adjustment of the North Atlantic sub-polar gyre $p\mathrm{CO}_2^o$.

The increase in North Atlantic $p\mathrm{CO}_2^o$ shown in Fig. 4B depends on the adjustment of the mean surface Revelle Buffer Factor R (panel D) [*Revelle and Suess*, 1957]. R measures the fractional ocean $p\mathrm{CO}_2$ change (denoted by δ) given a fractional change in DIC and vice versa such that

$$R = \frac{\delta pCO_2}{pCO_2} / \frac{\delta DIC}{DIC} \approx \frac{2 - Alk/DIC}{Alk/DIC - 1}, \tag{1}$$

where Alk is the Alkalinity. The Buffer Factor R quantifies the amount of carbon that can be stored in the form of DIC for a given change in atmospheric CO_2 concentration. High Buffer Factor systems are able to absorb changes in ocean $p\mathrm{CO}_2$ by storing carbon in the form of DIC. For example, in a high Buffer Factor region which absorbs atmospheric carbon, local DIC does not change significantly. Therefore more carbon remains in the form of dissolved CO_2, leading to higher $p\mathrm{CO}_2^o$ values and less uptake of atmospheric CO_2. The value of R can be approximated in terms of the ratio of Alkalinity over DIC, as shown in eqn. 1. As Alkalinity levels increase, the Buffer Factor decreases and the ocean becomes more capable of absorbing atmospheric CO_2 anomalies. Conversely, increasing DIC concentrations reduce the ocean's capacity to buffer atmospheric CO_2 changes.

Figure 4D shows that the temporal evolution of North Atlantic R corresponds to the change in North Atlantic $p\mathrm{CO}_2$ shown in panel B. Changes in the Buffer Factor account for 94% of the change in North Atlantic $p\mathrm{CO}_2$, while other changes such as temperature and salinity account for the remainder (using the approach of *Lovenduski et al.* [2007]). As a result of the increase in North Atlantic $p\mathrm{CO}_2$, the yearly air-sea flux of carbon in the region, $\overline{F_{air-sea}}$, is reduced compared to that of the control run (panel E). After roughly 425 years of the wind stress perturbation, the cumulative flux perturbation in the North Atlantic sub-polar region becomes zero such that the North Atlantic sub-polar region becomes a net emitter of carbon relative to the control state. The increase in Southern Ocean wind therefore induces a reduction in the North Atlantic carbon sink. The air-sea carbon flux in the Southern Ocean (panel F) also shows a long term decrease due to slow build up of atmospheric CO_2 driven by the North Atlantic, since the Southern Ocean $p\mathrm{CO}_2$ remains constant after 100 years of wind stress perturbation. After 400 years, the net change in the North Atlantic carbon flux is comparable in magnitude to the change in the Southern Ocean carbon flux.

3.2. Relative feedback of the North Atlantic on atmospheric CO_2

To quantify the strength of the non-local climate feedback on atmospheric $p\mathrm{CO}_2$ due to Southern Ocean wind stress, we compare it with the change in atmospheric CO_2 due to Southern Ocean outgassing, i.e. the local feedback. We define the non-local feedback parameter ϵ which relates a change in Southern Ocean $p\mathrm{CO}_2^o$, $\Delta\overline{pCO^o_{2SO}}$, to the subsequent change in North Atlantic $p\mathrm{CO}_2$, $\Delta\overline{pCO^o_{2NA}}$. If the $p\mathrm{CO}_2^o$ in the Southern Ocean is altered through changes in the large scale circulation and biogeochemistry, the perturbed ocean dynamical and biogeochemical state will also cause changes in the $p\mathrm{CO}_2$ elsewhere, such

as in the North Atlantic (as shown in Fig. 4). The relative changes in $p\mathrm{CO}_2$, $\Delta\overline{pCO^o_{2SO}}$ and $\Delta\overline{pCO^o_{2NA}}$ will therefore be related to one another:

$$\Delta\overline{pCO^o_{2NA}} = \epsilon\Delta\overline{pCO^o_{2SO}}. \quad (2)$$

We can use ϵ to express the atmospheric $p\mathrm{CO}_2$ anomaly, ΔpCO^a_2, due to a change in Southern Ocean $p\mathrm{CO}^o_2$, by considering the air-sea flux of carbon $F_{air-sea}$ over the global ocean. The air-sea flux equation takes the form [*Wanninkhof*, 1992]:

$$F_{air-sea} = k(pCO^a_2 - pCO^o_2), \quad (3)$$

where k is the gas transfer velocity. We integrate eqn. 3 over the global ocean. At equilibrium, the net air-sea flux is zero such that $\int F_{air-sea}dA = 0$. However, we split the integral into 3 different regions: the Southern Ocean, the North Atlantic sub-polar gyre, and the rest of the ocean basin, denoted by the subscripts SO, NA and E respectively. By considering a perturbation in atmospheric $p\mathrm{CO}_2$, ΔpCO^a_2, we can then write:

$$\Delta pCO^a_2 = (1 + \epsilon\frac{P_{NA}}{P_{SO}})P_{SO}\Delta\overline{pCO^o_{2SO}} + \Delta P_{SO}\overline{pCO^o_{2SO}} + \Delta P_{NA}\overline{pCO^o_{2NA}} + \Delta P_E\overline{pCO^o_{2E}} \quad (4)$$

where P_{SO}, P_{NA} and P_E are the area fractions of the respective regions, weighted by the local wind stress (see supplementary material). The first term in eqn. 4 is the change in atmospheric $p\mathrm{CO}_2$ due to changes in the ocean $p\mathrm{CO}_2$. In the case of $\epsilon = 0$, there would be no non-local effect and the change in atmospheric $p\mathrm{CO}_2$ would be due to change in Southern Ocean $p\mathrm{CO}_2$ alone. If ϵ is positive and takes a value of 1, the net feedback is positive and doubles the local Southern Ocean feedback on atmospheric $p\mathrm{CO}_2$, since P_{SO} are P_{NA} are roughly of equal magnitude. Conversely, if ϵ is negative with a value of -1, there would be an opposing non-local feedback which cancels out the local effect of the Southern Ocean wind stress. The second, third and fourth terms in eqn. 4 quantify

the change in atmospheric $p\mathrm{CO}_2$ due to the enhanced turbulent air-sea transfer of CO_2. However, these terms mostly cancel each other out and only account for $5-10\%$ of the total ΔpCO_2^a.

The value of ϵ can be estimated using both eqns. 2 and 4, since all terms apart from ϵ can be calculated and diagnosed from the MITgcm simulations. The results of the calculations are shown in Fig. 5. While there are differences in the results between using eqn. 2 and 4, the order of magnitude and trend of the calculated values of ϵ are similar. Values of ϵ are positive and range between 0.5 and 0.9 for weak wind stress perturbations. The magnitude of ϵ increases as the wind stress increases, ϵ is roughly 1.2 for a doubling of Southern Ocean wind stress. For all experiments, ϵ increases with time (not shown): from less than 0.4 in the first decade after the wind stress perturbation is initially applied to the quasi-equilibrium values of roughly 1 (as shown in Fig. 5). The climate feedback of Southern Ocean wind stress on atmospheric $p\mathrm{CO}_2$ is therefore almost doubled by the non-local effect. To understand the reason behind the change in the North Atlantic carbon sink, the following sections will describe the mechanism by which Southern Ocean winds influence the North Atlantic Buffer Factor, $\overline{R_{na}}$, and set the long-term centennial adjustment timescale of atmospheric $p\mathrm{CO}_2$ anomalies.

4. Southern Ocean winds, equatorial biology and the North Atlantic Buffer Factor

4.1. The effect of Southern Ocean winds on nutrient streams

In the Southern Ocean, surface biology is inefficient due to strong light and iron limitation [*Boyd et al.*, 2000; *Coale et al.*, 2004; *DeVries et al.*, 2012] such that the upwelled nutrients remain mostly unused. Instead, the nutrients are transported northwards and

into the ocean interior following the sub-surface currents in what are commonly referred to as nutrient streams [*Pelegri and Csanady*, 1991; *Pelegri et al.*, 1996, 2006; *Williams et al.*, 2006, 2011].

A nutrient stream is an advective pathway through which nutrients are transported from regions of upwelling and nutrient excess, such as the Southern Ocean, to nutrient-poor regions such as the equator and the Northern high latitudes (see Fig. 2D). The advective pathways mainly follow streamlines of the overturning circulation. Ekman transport drives nutrients northwards and out the Southern Ocean [*Williams and Follows*, 1998], where it is subducted below the mixed layer during the formation of Antarctic Intermediate Water. Transport is then predominantly isopycnal, with nutrients gradually re-inducted into the mixed layer as isopycnals shoal towards the surface in the North Atlantic sub-polar region [*Williams et al.*, 2006]. North of the Southern Ocean where biology is far more efficient, the nutrient stream causes an increase in macro nutrient-limited biological productivity [*Sarmiento et al.*, 2004]. The nutrient stream $S_P(x, y, z, t)$ is defined here as the meridional transport of Phosphorus, in the form of Phosphate PO_4^{3-}, by the meridional residual velocity field v and is given by

$$S_P(x, y, z, t) = \left[PO_4^{3-}\right] v, \tag{5}$$

where the square brackets indicate concentration. The zonally averaged nutrient stream S_P is shown in Fig. 2E for the MITgcm control run.

Physical transport in the ocean interior is mostly adiabatic along isopycnals, so the location of the nutrient stream lies along surfaces of constant density and its strength is modulated by the biological flux of nutrients [*Pelegri et al.*, 1996]. In the current numerical set-up, the maximum transport occurs along the potential density surface $\sigma_\theta = 26$ kg/m^3

(σ_{26}), shown in Fig. 2E for the control run. Therefore we interpolate the meridional transport of phosphate onto σ_{26}. Figure 6 shows the meridional nutrient transport, S_P, (panel A), the steady state concentration of PO_4^{3-} (panel B) along σ_{26} and the mean mixed layer biological productivity, F_{bio} (panel C). The spatial pattern of S_P shows the (positive) nutrient stream originating just north of the Southern channel where intermediate mode water is formed in region 1. The nutrient stream follows the northwards MOC transport along the western boundary in region 2, strengthening until it reaches the northern sub-polar gyre, where the nutrients are inducted back into seasonal thermocline in region 3.

The effect of increased Southern Ocean winds on the nutrient transport is shown in Figure 6 (bottom row) after 400 years of the $2 \times \tau_{SO}$ perturbation experiment. Due to the increase in Southern Ocean wind-induced vertical mixing, there is a global increase in concentrations of PO_4^{3-} along the perturbed $\sigma_\theta = 26$ kg/m^3 surface (σ'_{26}) in the Southern hemisphere (panel E). The wind stress perturbation also causes an increase in the meridional velocity v along σ'_{26}. As a result, there is an increase in the northwards nutrient stream (panel D). The increase in surface nutrients leads to additional nutrients being introduced into the nutrient-limited equatorial shadow zone in region 4 via eastward equatorial jets and mixing across the Southern shadow zone boundary. Subsequently, mixed layer biological productivity is strongly enhanced north of the Southern channel and in the eastern Tropics where nutrients are upwelled due to wind stress divergence (panel H). For the $2 \times \tau_{SO}$ experiment, the increase in biological productivity is less than 10% in the Southern channel, between 20% and 40% in the sub-polar gyre, but more than 200% between 20°S and 20°N. In the Northern sub-polar gyre, the response in biological pro-

ductivity is not as strong as in the Tropics. This relatively weak response in the sub-polar gyre is partly due to high-latitude light limitation [*Nielsdottir et al.*, 2009] and partly due to the depletion of the nutrient stream by the time it reaches the northern end of the basin. Most of the increase in biology is therefore centred around the eastern Tropics.

4.2. Surface biology and the Revelle Buffer Factor

An increase in equatorial biology can reduce atmospheric pCO_2 by drawing more carbon from the mixed layer to form biological tissue, therefore reducing ocean surface pCO_2^o and increasing the air-sea flux of carbon into the ocean. Conversely, it can increase atmospheric pCO_2 by affecting the chemistry of sub-thermocline waters in the shadow zone. Surface biology utilises DIC and Alkalinity at different rates. To understand the effect of biology on the Buffer Factor, let us consider the influence of mixed layer biology on the mixed layer chemistry. The key points discussed below are also summarised in the diagram in Fig. 7.

Production of soft matter reduces DIC by 117 moles for every mol of phosphate and increases Alkalinity by 16 moles, following Redfield stoichiometry [*Redfield*, 1934; *Anderson and Sarmiento*, 1994; *Weber and Deutsch*, 2012]. The formation or dissolution of 1 mol of calcite (hard tissue), on the other hand, reduces DIC by 1 mol and Alkalinity by 2 mol. Surface biology therefore changes the local concentrations of DIC and Alk depending on the relative export and remineralization of soft matter and calcite. The relative export of hard to soft matter, r, is known as the "rain ratio." Studies of climatological basin-wide and local seasonal data give a rain ratio between 0.05 and 0.1 in the open ocean, the former is used in the MITgcm experiments conducted here [*Sarmiento et al.*, 2002; *Jin*

et al., 2006; *Emerson et al.*, 2011]. For all values of r, an increase in surface biology results in a decrease of the relative ratio of DIC/Alk within the mixed layer.

Surface biology also affects the vertical transport of DIC and Alkalinity in the ocean. The soft matter that is produced in the ocean mixed layer falls through the water column until it is remineralized back into DIC, in the form of C_{soft}. The remineralisation of soft matter therefore increases DIC and reduces Alkalinity. Similarly, calcite shells produced in the mixed layer fall through the water column until they are dissolved into DIC in the form of C_{carb}. Dissolution of calcite increases DIC and Alkalinity. The remineralization depth of soft matter is shallower than hard tissue such that just below the mixed layer, remineralization of organic matter is mostly due to soft tissue which increases the relative ratio of DIC to Alk.

The relative concentration of DIC and Alkalinity of water parcels, influenced by surface biology, is pivotal for the climate system since they determine the value of the Revelle Buffer Factor R and therefore the capacity of the ocean to absorb atmospheric CO_2 (eqn. 1). In regions of high biological activity, surface waters are reduced in R and the underlying waters are therefore enhanced in R. If these water parcels are then advected away and upwelled at the surface elsewhere, they will increase R in the region of upwelling. Water parcels with an elevated Buffer Factor R will be less capable of absorbing atmospheric CO_2 anomalies, leading to a local reduction in the ocean carbon sink.

As Southern Ocean winds increase and surface biological productivity is enhanced across the global ocean, the strongest increase in the Buffer Factor R occurs below the thermocline in the equatorial shadow zone along σ'_{26} (Fig. 8), where the largest relative changes in DIC and Alk occur. After 50 years (panel A), there is an increase in R in the Southern

channel associated with increased upwelling of DIC-rich waters (region 1). A positive R anomaly occurs in the equatorial shadow zone due to the increased biological activity (region 2). After another 100 years (panel B), the anomaly in R in the Southern channel has decayed while the tropical anomaly signal intensified. Because ventilation of the shadow zone is sluggish compared to the rest of the ocean, the increase in the downward flux of organic matter from the surface causes a slow build up of DIC and a slow reduction of Alkalinity in the shadow zone leading to a rise of R-anomaly for centuries.

The increase in R generated in the Eastern Tropics is transported predominantly westward within the shadow zone through the equatorial current, where it is then entrained by the nutrient stream in the western boundary of the shadow zone. As shown in Fig. 8D, an additional recirculation of the R-anomaly within the shadow zone itself is present, leading to further advection towards the Southern edge of the shadow zone. After the R-anomaly is entrained into the nutrient stream, it follows the MOC transport northward (region 3) into the sub-tropical gyre where it is upwelled into the surface. The positive R-anomaly in the intermediate waters just North of the Southern Ocean, denoted by region 4 in Fig. 8C, is only 10% to 30% of the equatorial signal since the intermediate waters are ventilated at the surface prior to subduction.

4.3. Verification of the mechanism

The effects of Southern Ocean mixing and nutrient export on low- and high-latitude biological productivity have been extensively studied [*Anderson et al.*, 2002; *Sarmiento et al.*, 2004; *Marinov et al.*, 2006]. However, the advective pathways of biogeochemical tracers from the equatorial shadow zone to the North Atlantic and their impact on the subpolar gyre buffer factor are fairly novel. Therefore we run an additional experiment in

which we release a passive dye tracer into the shadow zone along σ'_{26} where concentrations of oxygen are less than 0.17 mol/m^3 in the control simulation (the oxygen minimum zone). Figure 9A shows the initial distribution of the tracer along σ'_{26}, while panels B and C show the dye concentration after 10 and 20 years, respectively. The tracer is being entrained near the western boundary and advected northwards towards the sub-polar gyre, where it is then mixed into the surface ocean. The advective timescale from the shadow zone to the North Atlantic sub-polar gyre is roughly 15 years.

Figures 8 and 9 show that the positive R anomaly from the shadow zone is advected to the North Atlantic sub-polar gyre. As discussed earlier, increases in surface biological activity in the sub-polar gyre can reduce the local mixed layer Buffer Factor. However, by the time the enhanced nutrient stream reaches the sub-polar gyre it is nearly stripped of the nutrient surplus so that the increase in biological activity in the North Atlantic sub-polar gyre is not sufficient to reduce the positive R-anomaly of the upwelled waters. The result is therefore an increase in the North Atlantic sub-polar gyre Buffer Factor due to the increased Southern Ocean wind stress.

Following this argument, the net change in the North Atlantic Buffer Factor $\overline{R_{na}}$ should depend on the relative change in the ratio of equatorial and North Atlantic biological productivity, such that

$$\overline{R_{na}} \propto \frac{\overline{F_{bio,eq}}}{\overline{F_{bio,na}}}, \tag{6}$$

where the overbar refers to the spatial averages between 10°S-10°N for the subscript "eq" and $40° - 60°$N for the subscript "na". Since an increase in the Buffer Factor $\overline{R_{na}}$ reduces the capacity of the North Atlantic to absorb atmospheric CO_2, we also expect that the

atmospheric $p\mathrm{CO}_2$, will scale with $\overline{R_{na}}$ such that

$$pCO_2^a \propto \overline{R_{na}}. \tag{7}$$

Using the MITgcm numerical simulations in which the wind stress is perturbed, we will explore the validity of eqns. 6 and 7. We run further simulations to explore the sensitivity of the results using wind stress perturbation experiments with a warmed spin-up state, with increased ocean stratification. The model is warmed by increasing the temperature restoring profile shown in Fig. 1C by 30% across the domain. The warmed model reaches a new equilibrium after 3000 years, at which time we introduce the same Southern Ocean wind stress perturbations described in section 2.2, up to a $3 \times \tau_{SO}$ perturbation.

Furthermore, experiments were also run whereby only the biogeochemical component in MITgcm is perturbed while keeping the wind stress profile constant. The parameters altered are the nutrient limitation half-saturation constant K_N [*Monod*, 1949] and the light limitation half-saturation constant I_k [*Jassby and Platt*, 1976]. The effect of perturbing the biogeochemical component is to increase or decrease biological activity by an amount which depends on the local light or nutrient limitation, without affecting the circulation so that the changes seen in $\overline{F_{bio,eq}}$ and $\overline{F_{bio,na}}$ are purely biogeochemical. Increasing K_N causes areas that were not limited in macro-nutrients (e.g. high latitudes) to become limited, effectively increasing $\frac{\overline{F_{bio,eq}}}{\overline{F_{bio,na}}}$. On the other hand, and increasing I_k reduces light limitation more at high latitudes compared to the Tropics, giving a reduction $\frac{\overline{F_{bio,eq}}}{\overline{F_{bio,na}}}$. The nutrient and light half-saturation perturbation experiments are designed to show that an increase in atmospheric $p\mathrm{CO}_2$ can also be caused by perturbations in the biology due to factors others than wind stress. The proposed feedback mechanism is therefore not solely dependent on Southern Ocean wind stress but can be caused by other climate change-

induced factors that affect surface biological activity, such as freshwater or micro-nutrient input.

The results for all numerical experiments to test eqns. 6 and 7 are shown in Fig. 10. Panel A shows that changes in $\frac{\overline{F_{bio,eq}}}{\overline{F_{bio,na}}}$ induce a linear change in $\overline{R_{na}}$ relative to the control state, $\Delta\overline{R_{na}}$, following the prediction of eqn. 6. The relationship is linear for perturbations less than 60% of the mean state. Furthermore, Fig. 10B shows that $\Delta p\mathrm{CO}_2^a$ varies linearly with $\Delta\overline{R_{na}}$ as predicted, where Δ indicates again the anomaly relative to the control state. The sensitivity of the atmospheric $p\mathrm{CO}_2^a$ anomaly to changes in the North Atlantic Buffer Factor in panel B depends on the control value of $p\mathrm{CO}_2^o$ and DIC concentration values, explaining the different slopes. The MITgcm experiments therefore show that an increase in tropical biological activity relative to Northern sub-polar gyre biological activity results in an increase in atmospheric $p\mathrm{CO}_2$, under a variety of wind stress and biogeochemical forcing scenarios.

5. Conclusion and Discussion

5.1. Summary of findings

The goal of this paper is to quantify the non-local equilibrium climate feedback of Southern Ocean wind stress on atmospheric $p\mathrm{CO}_2$, pCO_2^a, using idealised coarse-resolution MITgcm experiments. In addition to triggering local changes in Southern Ocean, an increase in the westerlies over the Southern Ocean can lead to changes in the biogeochemical and dynamical quantities in the Northern Hemisphere. Primarily, the North Atlantic carbon sink is found to be reduced several decades after an increase in Southern Ocean winds. The resulting feedback on atmospheric $p\mathrm{CO}_2$, measured by the non-local feedback parameter ϵ is of roughly the same order as the local Southern Ocean feedback. Overall, the non-local

effect of Southern Ocean wind stress perturbations on atmospheric $p\mathrm{CO}_2$ magnifies the local effect by 80% to 110%. The reduction in the North Atlantic carbon sink therefore constitutes a significant climate feedback that cannot be measured by considering changes in the Southern Ocean carbon sink alone.

Driving the reduction in the North Atlantic carbon sink is an increase in the Revelle Buffer Factor. It is found that wind stress-induced upwelling strengthens the export of nutrients north of the Southern Ocean by increasing the nutrient stream and increases equatorial biological productivity. The increased equatorial biological productivity increases the Revelle Buffer Factor, R, in the Eastern tropical shadow zone/oxygen minimum zone located between $100 - 700$m depth. Via ocean interior advective pathways, the waters enriched in R are entrained into the nutrient stream and transported to the North Atlantic where they are inducted into the seasonal thermocline, increasing the sub-polar gyre Buffer Factor and ocean $p\mathrm{CO}_2$, pCO_2^o. Due to the reduction in the North Atlantic carbon sink, atmospheric $p\mathrm{CO}_2$ is increased. The mechanism is also verified by only perturbing the biogeochemical component of the model.

5.2. Caveats and Implications

The use of a coarse-resolution model introduces several caveats. Coarse-resolution models fail to accurately represent the extent of the oxygen-minimum zones. Due to the unresolved complexity in equatorial undercurrents, a phenomenon coined "nutrient trapping" [*Najjar*, 1990; *Aumont et al.*, 1999] results in overestimation of the strength of the oxygen minimum in the Tropics. Nonetheless, the proposed mechanism should still be valid since oxygen minimum zones are observed in the ocean [*Stramma et al.*, 2009]. However, nutrient trapping could amplify the strength of the non-local feedback due to a exagger-

ated biogeochemical response in the tropics. Unresolved eddies in the Southern Ocean also overestimate the wind stress-induced increase in nutrient upwelling, since a constant GM coefficient is used the model. However, both Southern Ocean pCO_2^o and the relative response of the North Atlantic and Equatorial biology depend equally on upwelling in the Southern Ocean so we don't expect this to affect the relative magnitude of the non-local feedback, although it may affect the equilibration timescale. For a full appreciation of the effect of eddies, a high resolution eddy-permitting or eddy-resolving simulation is required.

Lastly, the geometry of the sector model introduces several caveats: the size of the basin plays an important role in setting the equilibration timescale of the non-local Southern Ocean winds feedback on $p\mathrm{CO}_2^a$. The feedback equilibration timescale depends on basin-wide advection: the Buffer Factor anomaly in the shadow zone has to be advected zonally from East to West across a larger oxygen minimum zone before it is advected northwards by the nutrient steam. To illustrate this dependence of the timescale on basin width, an identical MITgcm set up 40° in longitude wide is used where the equilibration takes twice as long in the 40° longitude model (see supplementary material). However, the strength of the non-local feedback ϵ is similar. The width of the basin therefore determines the timescale of the non-local feedback but not the magnitude. Further study is required to determine the exact equilibration timescale with a realistic geometry. The model also lacks a Pacific and Indian Ocean. However, the lack of MOC-like large scale overturning transport and lack of strong ocean carbon uptake in the Pacific and Indian basins means that the presence of these basins will not affect the magnitude of the feedback of Southern Ocean winds on atmospheric CO_2 via the North Atlantic sub-polar gyre. The increase

in biological carbon drawdown in the Pacific and Indian basins as a result of increased nutrient transport is likely to be small due to the simultaneous input of surface carbon.

The relationship between the North Atlantic Buffer Factor and equatorial biology has further implications for the climate as well, since the ratio of North Atlantic to Equatorial biology can be altered by many processes such as stratification, cloud cover, other sources of macro-nutrients, iron supply, to name a few. Our results show the influence of oxygen-minimum zones on North Atlantic surface chemistry. Given recent results from studies that show expansion of tropical oxygen-minimum zones [*Stramma et al.*, 2012], a thorough understanding of the biogeochemical drivers of the North Atlantic Buffer Factor is therefore needed. The North Atlantic sub-polar region constitutes one of the main sinks for anthropogenic CO_2 and our results shows that changes in the Buffer Factor of as small as 0.5 could result in a positive atmospheric carbon feedback of $10 - 30$ppm.

Furthermore, Southern Ocean winds and vertical mixing have been used to partially explain glacial-interglacial cycles of atmospheric CO_2. *Francois et al.* [1997] and *Anderson et al.* [2009] suggest that there was an increase in vertical mixing in the Southern Ocean at end of the Last Glacial Maximum (LGM), 20000-12000 years before present, possibly related to an increase in wind stress. So far however, current theories of physical mechanisms have not been able to fully explain the glacial-interglacial cycles of atmospheric CO_2 [*Sigman and Boyle*, 2000; *Solomon*, 2007]. Including the effects of the non-local atmospheric feedback of the North Atlantic due to Southern Ocean vertical mixing could aid our understanding of glacial-interglacial atmospheric CO_2 cycles.

Kohfeld et al. [2005] show that there was higher biological carbon export in the Atlantic equatorial shadow zone in the LGM but states that "these areas are relatively small and

do not affect the overall picture," while our research shows these areas should not be overlooked. Although global changes in ocean alkalinity have been acknowledged as being potentially important, there has been no consideration of spatial patterns. *Kohfeld et al.* [2005] does not give exact figures of the relative change in biological export in the Tropics and North Atlantic. However, *Francois et al.* [1997] suggest that Southern Ocean vertical mixing was increased by 20% to 50% at the end of the LGM, which, given our model study, would correspond to an increase in atmospheric $p\mathrm{CO}_2$ of 15-35 ppm in addition to the local Southern Ocean outgassing.

Acknowledgments. BB was supported by a NERC CASE studentship with the Met Office. Further support from NERC was provided to LZ and DRM. This work made use of the facilities of HECToR and Archer. We acknowledge the MITgcm team for making their code publicly available. We would also like to thank the reviewers for their helpful suggestions and comments. Details and results from the numerical simulations are available from BB.

References

Anderson, L., and J. Sarmiento (1994), Redfield Ratios Of Remineralization Determined By Nutrient Data-Analysis, *Global Biogeochemical Cycles*, *8*(1), 65–80, doi:10.1029/93GB03318.

Anderson, R., Z. Chase, M. Fleisher, and J. Sachs (2002), The Southern Ocean's biological pump during the Last Glacial Maximum, *Deep-Sea Research Part Ii-Topical Studies In Oceanography*, *49*(9-10), 1909–1938, doi:10.1016/S0967-0645(02)00018-8.

Anderson, R. F., S. Ali, L. I. Bradtmiller, S. H. H. Nielsen, M. Q. Fleisher, B. E. Anderson, and L. H. Burckle (2009), Wind-Driven Upwelling in the Southern Ocean and the Deglacial Rise in Atmospheric CO2, *Science*, *323*(5920), 1443–1448, doi:10.1126/science.1167441.

Aumont, O., J. Orr, P. Monfray, G. Madec, and E. Maier-Reimer (1999), Nutrient trapping in the equatorial Pacific: The ocean circulation solution, *Global Biogeochemical Cycles*, *13*(2), 351–369.

Boyd, P. W., , and et. al. (2000), A mesoscale phytoplankton bloom in the polar southern ocean stimulated by iron fertilisation, *Nature*, *407*.

Bracegirdle, T. J., E. Shuckburgh, J.-B. Sallee, Z. Wang, A. J. S. Meijers, N. Bruneau, T. Phillips, and L. J. Wilcox (2013), Assessment of surface winds over the atlantic, indian and pacific ocean sectors of the southern ocean in cmip5 models: historical bias, forcing response and state dependence, *Journal of Geophysical Research*, *118*.

Brandt, P., H. W. Bange, D. Banyte, M. Dengler, S. H. Didwischus, T. Fischer, R. J. Greatbatch, J. Hahn, T. Kanzow, J. Karstensen, A. Kroertzinger, G. Krahmann, S. Schmidtko, L. Stramma, T. Tanhua, and M. Visbeck (2015), On the role of circulation and mixing in the ventilation of oxygen minimum zones with a focus on the eastern tropical North Atlantic, *BIOGEOSCIENCES*, *12*(2), 489–512, doi:10.5194/bg-12-489-2015.

Coale, K. H., , and et. al. (2004), Southern ocean iron enrichment experiment: carbon cycling in high- and low-si waters, *Science*, *304*.

DeVries, T., F. Primeau, and C. Deutsch (2012), The sequestration efficiency of the biological pump, *Geophysical Research Letters*, *39*.

Dickson, R. R., J. Meincke, and P. Rhines (2008), Arctic-subarctic ocean fluxes - defining the role of the northern seas in climate, *Springer*.

Dutkiewicz, S., M. Follows, and P. Parekh (2008), Interactions of the iron and phosphorus cycles: a three-dimensional model study, *Global Biogeochemical Cycles*, *19*.

Emerson, S., C. Sabine, M. F. Cronin, R. Feely, S. E. C. Gray, and M. DeGrandpre (2011), Quantifying the flux of CaCO3 and organic carbon from the surface ocean using in situ measurements of O-2, N-2, pCO(2), and pH, *Global Biogeochemical Cycles*, *25*, doi: 10.1029/2010GB003924.

Feely, R. A., C. L. Sabine, T. Takahashi, and R. Wanninkhof (2001), Uptake and storage of carbon dioxide in the oceans: The global co2 survey, *Oceanography*, *14*.

Firing, E., S. Wijffels, and P. Hacker (1998), Equatorial subthermocline currents across the Pacific, *Journal Of Geophysical Research-Oceans*, *103*(C10), 21,413–21,423, doi: 10.1029/98JC01944.

Follows, M. J., T. Ito, and S. Dutkiewicz (2006), On the solution of the carbonate chemistry system in ocean biogeochemistry models, *Ocean Modeling*, *12*.

Francois, R., M. Altabet, E. Yu, D. Sigman, M. Bacon, M. Frank, G. Bohrmann, G. Bareille, and L. Labeyrie (1997), Contribution of Southern Ocean surface-water stratification to low atmospheric CO2 concentrations during the last glacial period, *Nature*, *389*(6654), 929–935, doi:10.1038/40073.

Gent, P., and McWilliams (1990), Isopycnal mixing in ocean circulation models, *Journal of Physical Oceanography*, *20*.

Gnanadesikan, A. (1999), A simple predictive model for the structure of the oceanic pycnocline, *Science*, *283*(5410), 2077–2079, doi:10.1126/science.283.5410.2077.

Group, T. L. S. (1998), The labrador sea deep convection experiment., *Bull. Amer. Meteor. Soc.*, *79*.

Gruber, N. (1998), Anthropogenic co2 in the atlantic ocean, *Global Biogeochemical Cycles*, *12*.

Halloran, P. R., B. B. B. Booth, C. D. Jones, F. H. Lambert, D. J. McNeall, I. J. Totterdell, and C. Voelker (2015), The mechanisms of North Atlantic CO_2 uptake in a large Earth System Model ensemble, *Biogeosciences*, *12*.

Ito, T., and M. J. Follows (2003), Upper ocean control on the solubility pump of co2, *Journal of Marine Research*, *61*.

Ito, T., and M. J. Follows (2005), Preformed phosphate, soft tissue pump and atmospheric co2, *Journal of Marine Research*, *63*.

Ito, T., M. Woloszyn, and M. Mazloff (2010), Anthropogenic carbon dioxide transport in the Southern Ocean driven by Ekman flow, *Nature*, *463*(7277), 80–U85, doi: 10.1038/nature08687.

Izumo, T., J. Picaut, and B. Blanke (2002), Tropical pathways, equatorial undercurrent variability and the 1998 La Nina, *Geophysical Research Letters*, *29*(22), doi: 10.1029/2002GL015073.

Jassby, A., and T. Platt (1976), Mathematical Formulation Of Relationship Between Photosynthesis And Light For Phytoplankton, *Limnology And Oceanography*, *21*(4), 540–547.

Jin, X., N. Gruber, J. P. Dunne, J. L. Sarmiento, and R. A. Armstrong (2006), Diagnosing the contribution of phytoplankton functional groups to the production and export of particulate organic carbon, CaCO3, and opal from global nutrient and alkalinity distributions, *Global Biogeochemical Cycles*, *20*(2), doi:10.1029/2005GB002532.

Key, R., A. Kozyr, C. Sabine, K. Lee, R. Wanninkhof, J. Bullister, R. Feely, F. Millero, C. Mordy, and T. Peng (2004), A global ocean carbon climatology: Results from Global Data Analysis Project (GLODAP), *GLOBAL BIOGEOCHEMICAL CYCLES*, *18*(4), doi:10.1029/2004GB002247.

Khatiwala, S., F. Primeau, and T. Hall (2009), Reconstruction of the history of anthropogenic co2 concentrations in the ocean, *Nature*, *462*.

Kieke, D., and I. Yashayaev (2014), Studies of labrador sea water formation and variability in the sub polar north atlantic in the light of international partnership and collaboration, *Progress in Oceanography*, *79*.

Knauss, J. (1960), Measurements Of The Cromwell Current, *Deep-Sea Research*, *6*(4), 265–286.

Kohfeld, K., C. Le Quere, S. Harrison, and R. Anderson (2005), Role of marine biology in glacial-interglacial CO2 cycles, *Science*, *308*(5718), 74–78, doi:10.1126/science.1105375.

Lauderdale, J. M., A. C. N. Garabato, K. I. C. Oliver, M. J. Follows, and R. G. Williams (2013), Wind-driven changes in Southern Ocean residual circulation, ocean carbon reservoirs and atmospheric CO2, *Climate Dynamics*, *41*(7-8), 2145–2164, doi: 10.1007/s00382-012-1650-3.

Le Quere, C., C. Rodenbeck, E. T. Buitenhuis, T. J. COnway, R. Langenfelds, A. Gomez, C. Labuschagne, M. Ramonet, T. Nakazawa, N. Metzl, N. Gillett, and M. Heimann (2007), Saturation of the souther ocean co2 sink due to recent climate changes, *Science*, *22*.

Lovenduski, N., and T. Ito (2009), The future evolution of the southern ocean co2 sink, *Journal of Marine Research*, *67*.

Lovenduski, N. S., N. Gruber, S. C. Doney, and I. D. Lima (2007), Enhanced CO2 outgassing in the Southern Ocean from a positive phase of the Southern Annular Mode, *Global Biogeochemical Cycles*, *21*(2), doi:10.1029/2006GB002900.

Lovenduski, N. S., N. Gruber, and S. C. Doney (2008), Toward a mechanistic understanding of the decadal trends in the Southern Ocean carbon sink, *Global Biogeochemical Cycles*, *22*(3), doi:10.1029/2007GB003139.

Marinov, I., A. Gnanadesikan, J. Toggweiler, and J. Sarmiento (2006), The Southern Ocean biogeochemical divide, *Nature*, *441*(7096), 964–967, doi:10.1038/nature04883.

Marshall, J., and T. Radko (2003), Residual-mean solutions for the antarctic circumpolar current and its associated overturning circulation, *Journal of Physical Oceanography*.

Marshall, J., and K. Speer (2012), Closure of the meridional overturning circulation through Southern Ocean upwelling, *NATURE GEOSCIENCE*, *5*(3), 171–180, doi: 10.1038/NGEO1391.

Marshall, J., A. Adcroft, C. Hill, L. Perelman, and C. Heisey (1997), A finite-volume, incompressible navier stokes model for studies of the ocean on parallel computers, *Journal of Geophysical Research - Oceans*, *102*.

Monod, J. (1949), The Growth Of Bacterial Cultures, *Annual Review Of Microbiology*, *3*, 371–394, doi:10.1146/annurev.mi.03.100149.002103.

Munday, D. R., H. L. Johnson, and D. P. Marshall (2013), Eddy saturation of equilibrated circumpolar currents, *Journal of Physical Oceanography*, *43*.

Munday, D. R., H. L. Johnson, and D. P. Marshall (2014), Impacts and effects of mesoscales eddies on ocean carbon storage and atmospheric pco2, *Global Biogeochemical Cycles*, *28*.

Najjar, R. G. (1990), Simulations of the phosphorus and oxygen cycles in the world ocean using a general circulation model, *Phd. Thesis, Princeton University, Princeton N. J.*

Nielsdottir, M. C., C. M. Moore, R. Sanders, D. J. Hinz, and E. P. Achterberg (2009), Iron limitation of the postbloom phytoplankton communities in the Iceland Basin, *Global Biogeochemical Cycles*, *23*, doi:10.1029/2008GB003410.

Palter, J. B., J. L. Sarmiento, A. Gnanadesikan, J. Simeon, and R. D. Slater (2010), Fueling export production: nutrient return pathways from the deep ocean and their dependence on the meridional overturning circulation, *Biogeosciences*, *7*(11), 3549–3568, doi:10.5194/bg-7-3549-2010.

Pelegri, J. L., and G. T. Csanady (1991), Nutrient transport and mixing in the gulf stream, *Journal of Geophysical Research*, *96*.

Pelegri, J. L., G. T. Csanady, and A. Martins (1996), The north atlantic nutrient stream, *Journal of Oceanography*, *52*.

Pelegri, J. L., A. MArrero-Diaz, and A. W. Ratsimandresy (2006), Nutrient irrigation of the north atlantic, *Progress in Oceanography*, *70*.

Philander, S. (1973), Equatorial Undercurrent - Measurements And Theories, *Reviews Of Geophysics*, *11*(3), 513–570, doi:10.1029/RG011i003p00513.

Philander, S., W. Hurlin, and A. Seigel (1987), Simulation Of The Seasonal Cycle Of The Tropical Pacific-Ocean, *Journal Of Physical Oceanography*, *17*(11), 1986–2002, doi:10.1175/1520-0485(1987)017¡1986:SOTSCO¿2.0.CO;2.

Qiu, B., D. L. Rudnick, S. Chen, and Y. Kashino (2013), Quasi-stationary North Equatorial Undercurrent jets across the tropical North Pacific Ocean, *Geophysical Research Letters*, *40*(10), 2183–2187, doi:10.1002/grl.50394.

Redfield, A. (1934), On the proportions of organic derivatives in sea water and their relation to the composition of plankton, *In Daniel, R.J. (ed James Johnstone Memorial Volume) University Press of Liverpool*, p. 177192.

Revelle, R., and H. S. Suess (1957), Carbon dioxide exchange between atmosphere and ocean and the the questions of an increase of atmospheric co2 during the past decades,

Tellus.

Rowe, G., E. Firing, and G. Johnson (2000), Pacific equatorial subsurface countercurrent velocity, transport, and potential vorticity, *Journal Of Physical Oceanography*, *30*(6), 1172–1187, doi:10.1175/1520-0485(2000)030¡1172:PESCVT¿2.0.CO;2.

Sarmiento, J., J. Dunne, A. Gnanadesikan, R. Key, K. Matsumoto, and R. Slater (2002), A new estimate of the CaCO3 to organic carbon export ratio, *Global Biogeochemical Cycles*, *16*(4), doi:10.1029/2002GB001919.

Sarmiento, J. L., N. Gruber, M. A. Brzezinski, and J. P. Dunne (2004), High-latitude controls of thermocline nutrients and low latitude biological productivity, *Nature*.

Sigman, D., and E. Boyle (2000), Glacial/interglacial variations in atmospheric carbon dioxide, *Nature*, *407*(6806), 859–869, doi:10.1038/35038000.

Solomon, S. (2007), *Climate change 2007-the physical science basis: Working group I contribution to the fourth assessment report of the IPCC*, vol. 4, Cambridge University Press.

Stramma, L., M. Visbeck, P. Brandt, T. Tanhua, and D. Wallace (2009), Deoxygenation in the oxygen minimum zone of the eastern tropical north atlantic, *Geophysical Research Letters*, *36*.

Stramma, L., E. D. Prince, S. Schmidtko, J. Luo, J. P. Hoolihan, M. Visbeck, D. W. R. Wallace, P. Brandt, and A. Koertzinger (2012), Expansion of oxygen minimum zones may reduce available habitat for tropical pelagic fishes, *Nature Climate Change*, *2*(1), 33–37, doi:10.1038/NCLIMATE1304.

Swart, N. C., J. C. Fyfe, O. A. Saenko, and M. Eby (2014), Wind-driven changes in the ocean carbon sink, *Biogeosciences*, *11*.

Takahashi, T., , and et. al. (2009), Climatological mean and decadal change in surface ocean pco2 and net sea-air co2 flux over the global oceans, *Deep Sea Research II*, *56*.

Tsuchiya, M. (1972), Subsurface North Equatorial Countercurrent In Eastern Pacific Ocean, *Journal Of Geophysical Research*, *77*(30), 5981–&, doi: 10.1029/JC077i030p05981.

Valsala, V., and S. Maksyutov (2010), Simulation and assimilation of global ocean pCO(2) and air-sea CO2 fluxes using ship observations of surface ocean pCO(2) in a simplified biogeochemical offline model, *Tellus Series B-Chemical And Physical Meteorology*, *62*(5, SI), 821–840, doi:10.1111/j.1600-0889.2010.00495.x.

Wanninkhof, R. (1992), Relationship between wind speed and gas exchange over the ocean, *Journal of Geophysical Research: Oceans*, *97*.

Weber, T., and C. Deutsch (2012), Oceanic nitrogen reservoir regulated by plankton diversity and ocean circulation, *Nature*.

Williams, R., and M. Follows (1998), The Ekman transfer of nutrients and maintenance of new production over the North Atlantic, *Deep-Sea Research Part I-Oceanographic Research Papers*, *45*(2-3), 461–489, doi:10.1016/S0967-0637(97)00094-0.

Williams, R. G., and M. Follows (2011), *Ocean Dynamics and the carbon cycle: principles and mechanics*, Cambridge University Press.

Williams, R. G., V. Roussenov, and M. J. Follows (2006), Nutrient streams and their induction into the mixed layer, *Global Biogeochemical Cycles*, *20*.

Williams, R. G., E. McDonagh, V. Roussenov, S. Torres-Valdes, B. King, R. Sanders, and D. A. Hansel (2011), Nutrient streams in the north atlantic: Advective pathways of inorganic and dissolved organic nutrients, *Global Biogeochemical Cycles*, *25*.

Wolfe, C., and P. Cessi (2010), What sets the strength of the midddepth stratification and overturning circulation in eddying ocean models?, *Journal of Physical Oceanography*, *40*.

Wyrtki, K., and B. Kilonsky (1984), Mean Water And Current Structure During The Hawaii-To-Tahiti Shuttle Experiment, *Journal Of Physical Oceanography*, *14*(2), 242–254, doi:10.1175/1520-0485(1984)014¡0242:MWACSD¿2.0.CO;2.

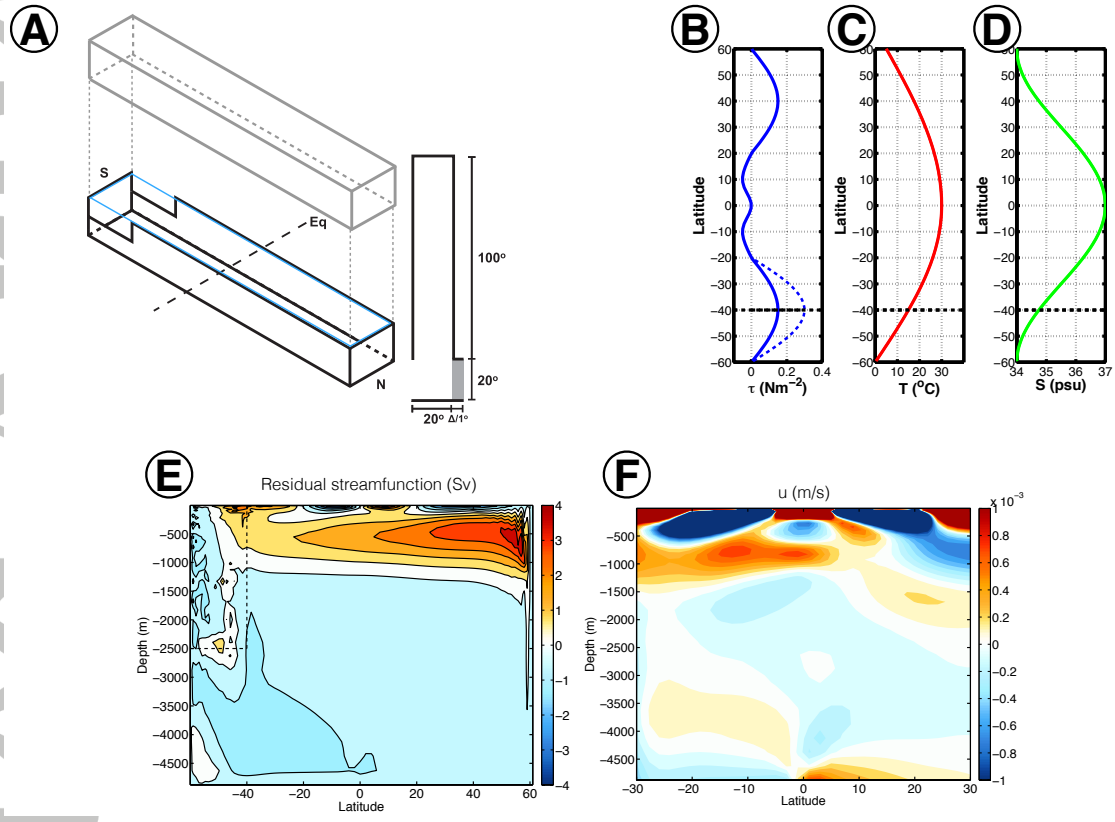

Figure 1. A) Schematic of MITgcm sector. Latitudinal profiles of surface boundary conditions for the control experiment of B) wind, with the dashed line showing a $2 \times \tau_{SO}$ perturbation, C) temperature and D) salinity. Control experiment steady state E) residual overturning streamfunction and F) zonal mean velocity.

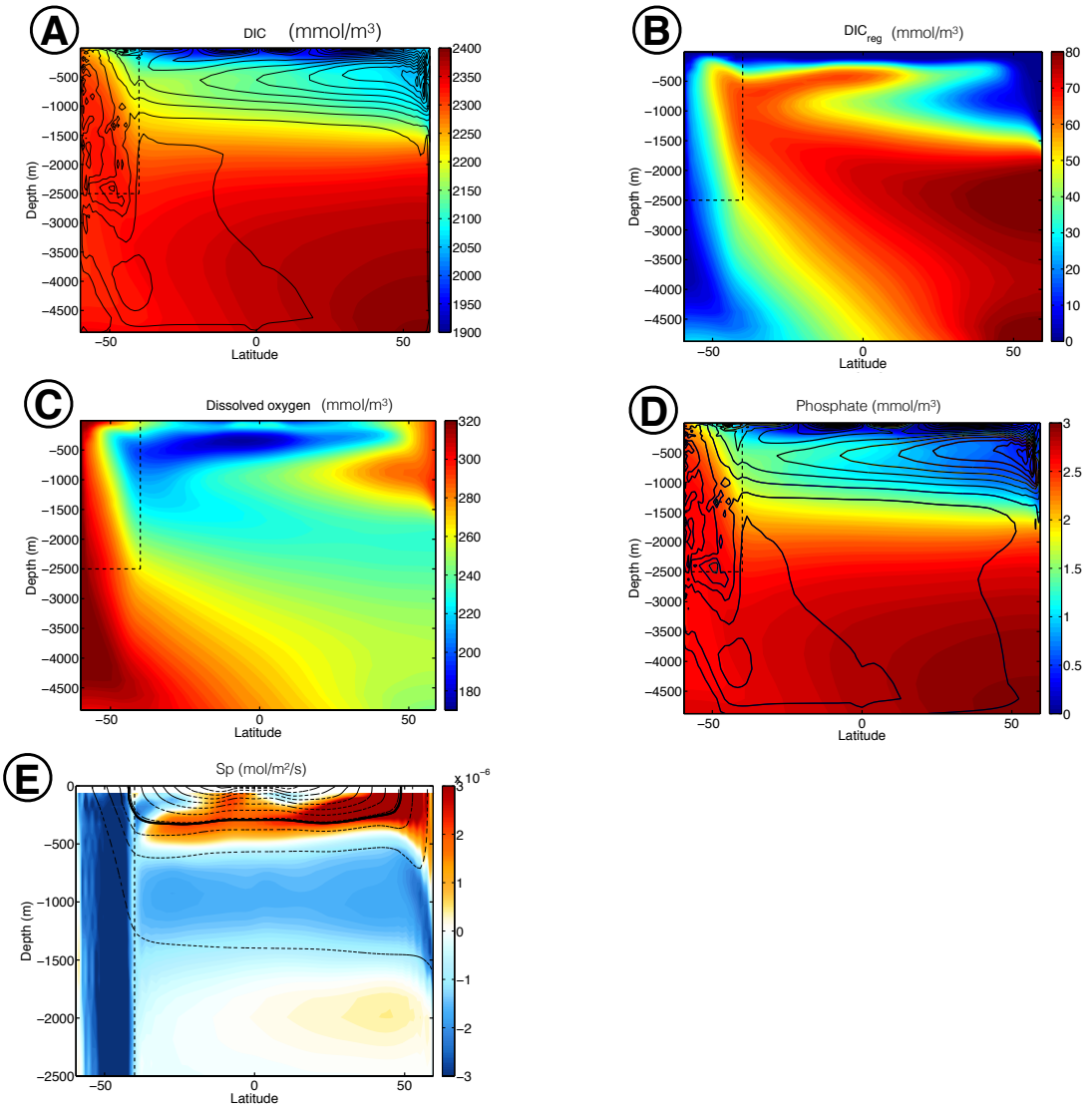

Figure 2. Zonally averaged A) total Dissolved Inorganic Carbon, B) regenerated Dissolved Inorganic Carbon, C) dissolved oxygen, D) dissolved phosphate. Dashed black lines in A-D indicate the extent of the channel and the solid black lines are residual overturning stream function contours spaced 1Sv apart. E) Zonally averaged meridional nutrient stream as defined by eqn. 5, with dashed lines showing surfaces of constant density and the thick black line showing the $\sigma_\theta = 26$ kg/m^3 density surface.

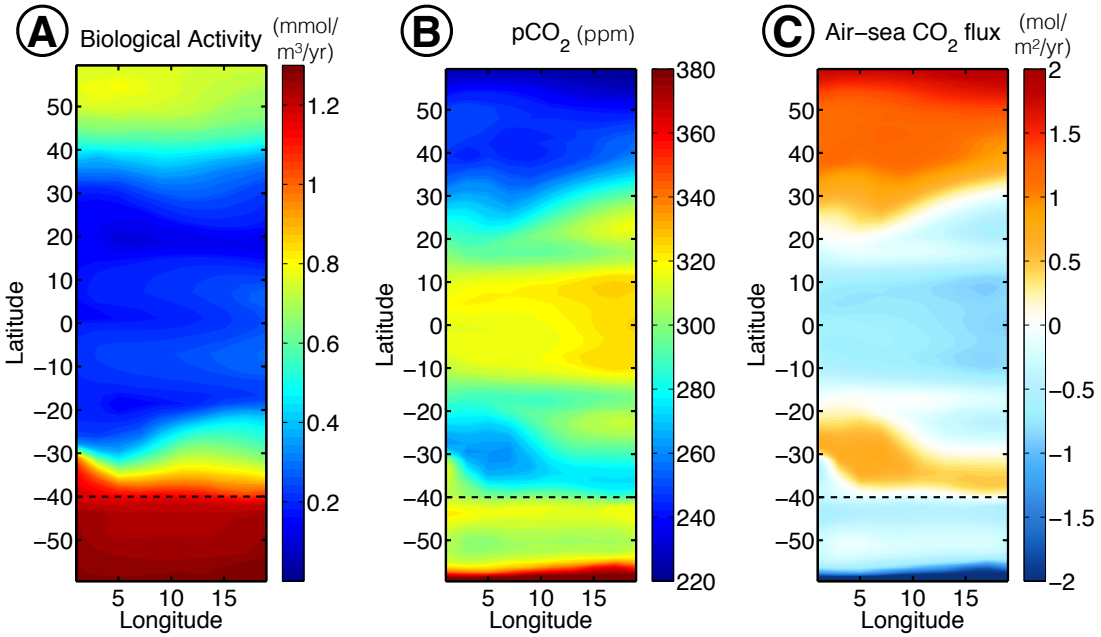

Figure 3. Steady state biogeochemical quantities in the control experiment: A) Mixed layer average biological activity (mmol/m^3/year of Phosphate), B) Mixed Layer Ocean pCO_2 and C) Air-sea CO_2 flux. Dashed black lines indicate the extent of the channel.

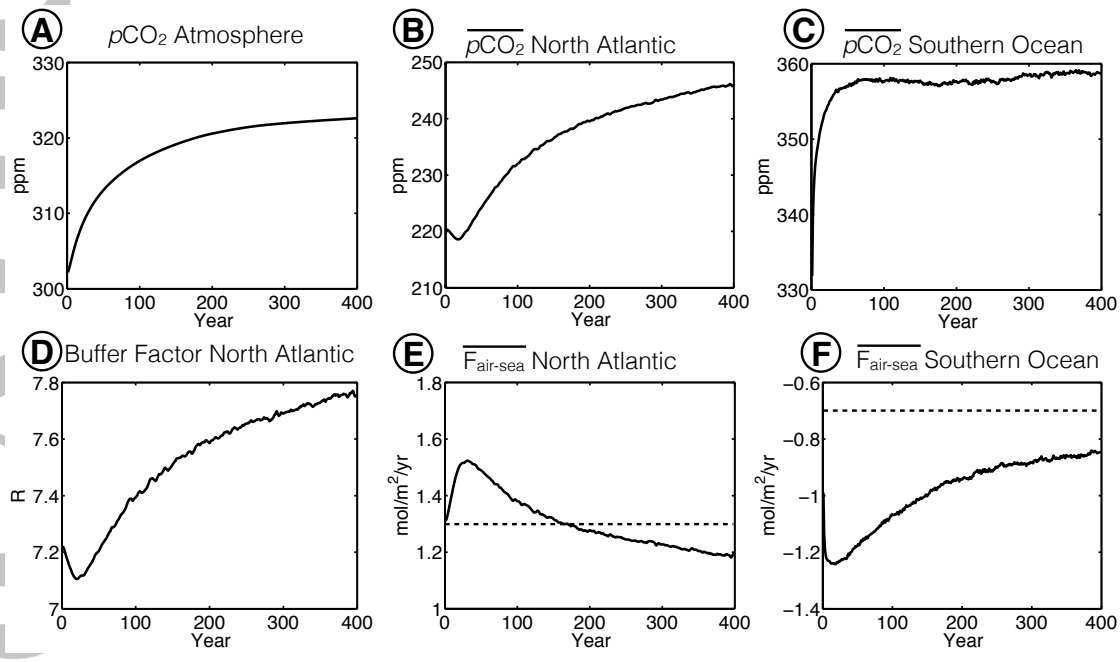

Figure 4. Time evolution of A) Southern Ocean mean surface pCO_2^o, B) North Atlantic subpolar gyre mean surface pCO_2^o, C) atmospheric pCO_2^a, D) North Atlantic mean surface Revelle Buffer Factor, E) North Atlantic and F) Southern Ocean net air-sea flux of carbon, in the $2 \times \tau_{SO}$ experiment. The dashed lines in panel E and F show the control mean air-sea flux. The overline indicates a spatial mean between $40° - 60°$N and $40° - 60°$S for the North Atlantic and Southern Ocean respectively.

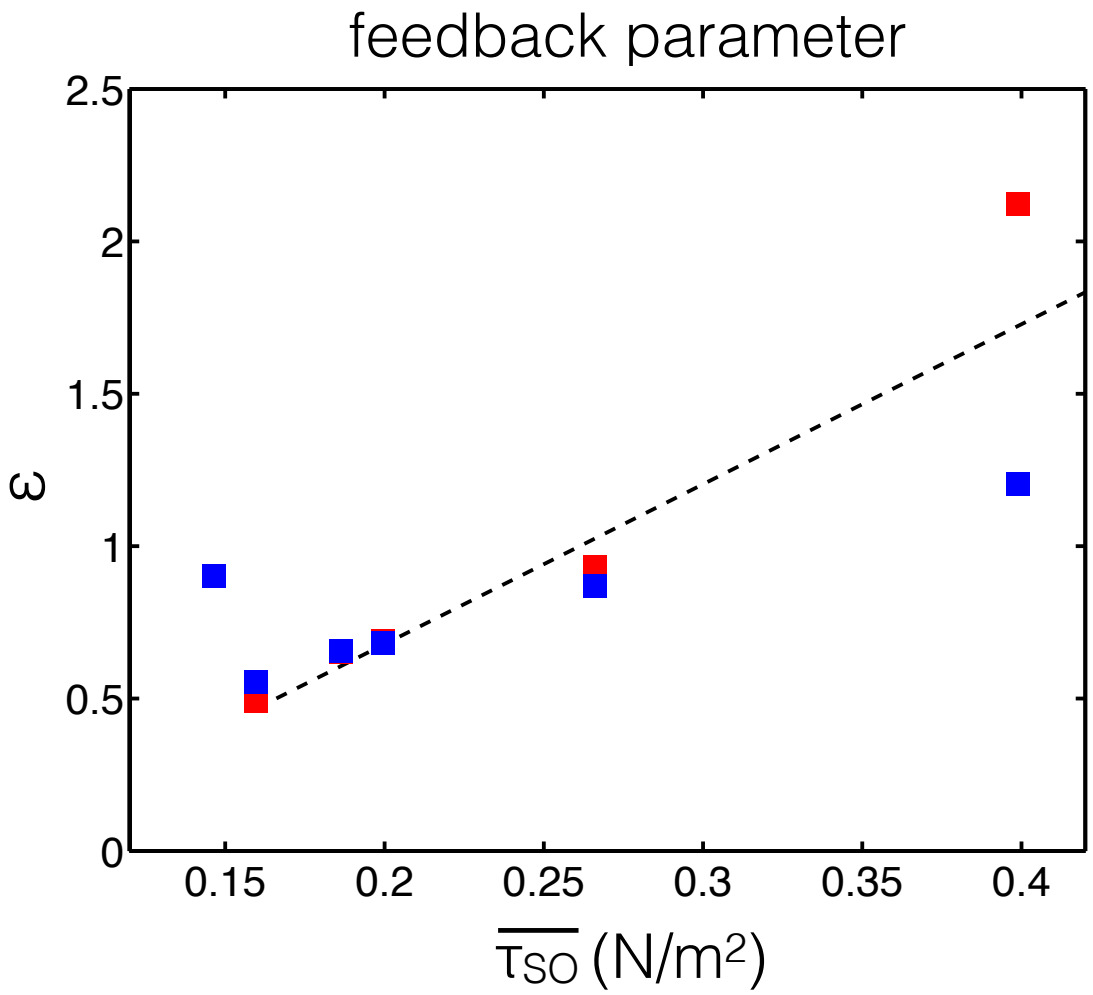

Figure 5. The feedback parameter ϵ as a function of wind stress in MITgcm estimated using eqns. 2 (blue) and 4 (red). The black line shows the linear trend.

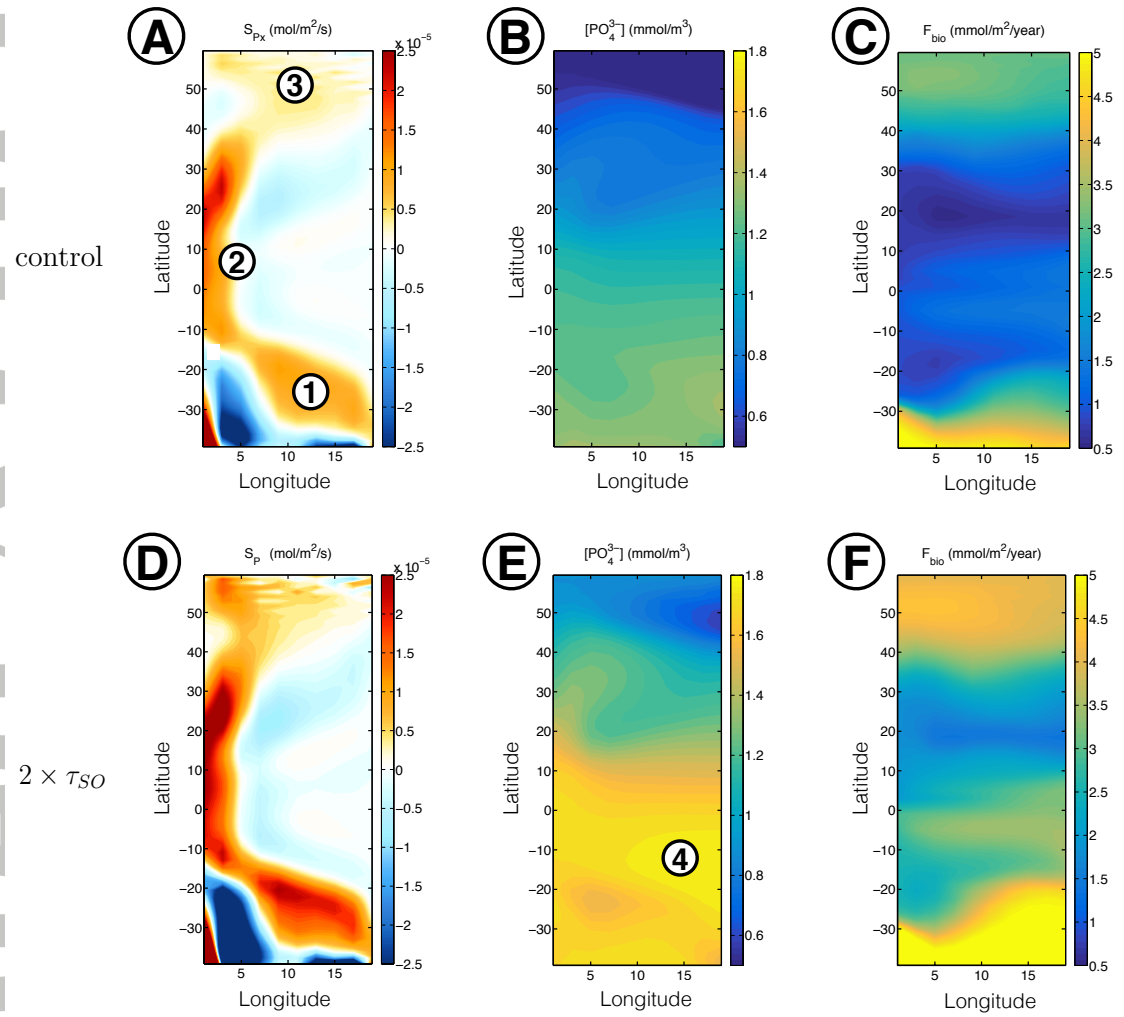

Figure 6. The nutrient stream S_p (A, D), phosphorous (B, E) on the $\sigma_\theta = 26$ kg/m^3 surface and the mean mixed layer biological productivity (C, F). Top row is for the control run and bottom row is after 400 years of a $2 \times \tau_{SO}$ perturbation. Only fields North of the Southern channel are shown for clarity.

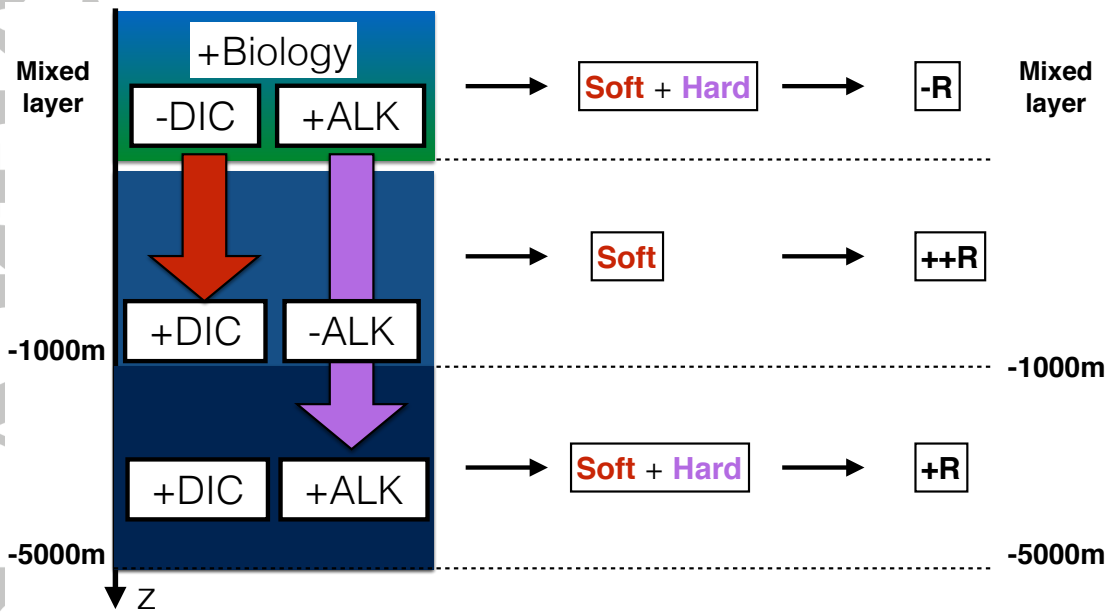

Figure 7. Diagram of the influence of surface biology on the Revelle Buffer Factor R. As mixed layer biological activity increases, mixed layer DIC is reduced and Alkalinity is increased, lowering the Buffer Factor. Underneath the mixed layer to roughly 1000m depth, more soft matter is remineralized compared to hard tissue, leading to an increase in DIC and a reduction of Alkalinity, resulting in a strong increase in the Buffer Factor. Deep in the water column, remineralization of soft and hard tissue is comparable giving an increase in both DIC and Alkalinity, resulting in a more moderate increase in the Buffer Factor.

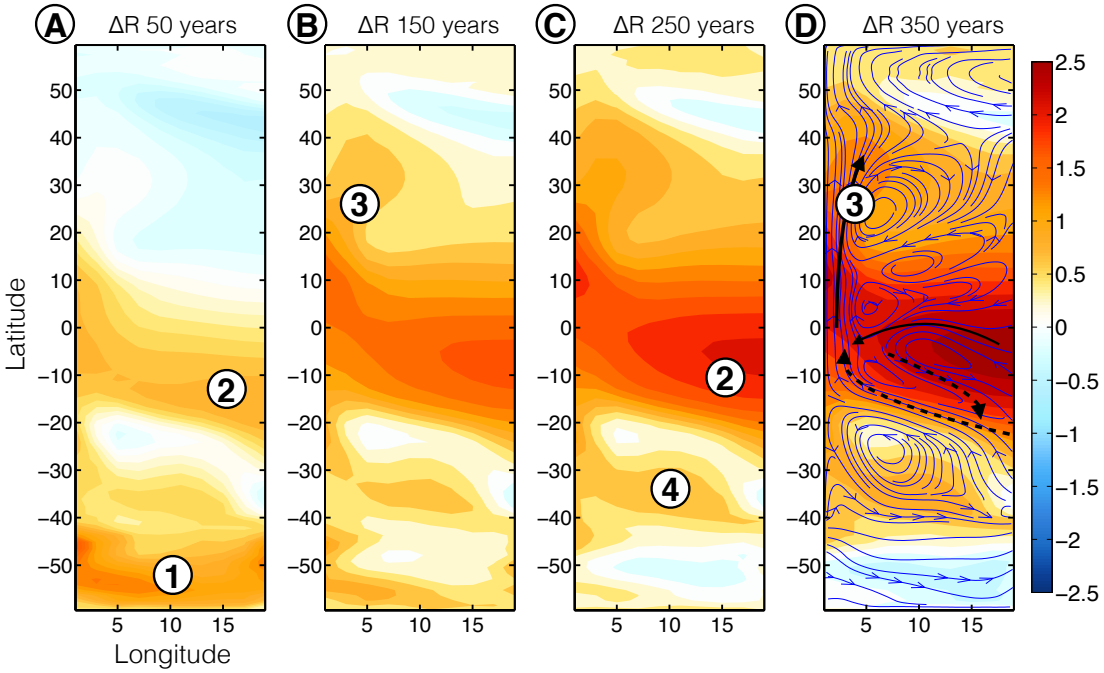

Figure 8. Revelle Buffer Factor anomaly ($2 \times \tau_{SO}$ - control) along the perturbed $\sigma_\theta = 26$ kg/m^3 surface after A) 50, B) 150, C) 250 and D) 400 years. The blue arrows in panel D show the perturbed flow field along the σ'_{26} surface. The black arrows shows the primary advection pathway out of the equatorial shadow zone, while the dashed arrows show a secondary advection pathway due to recirculation within the shadow zone.

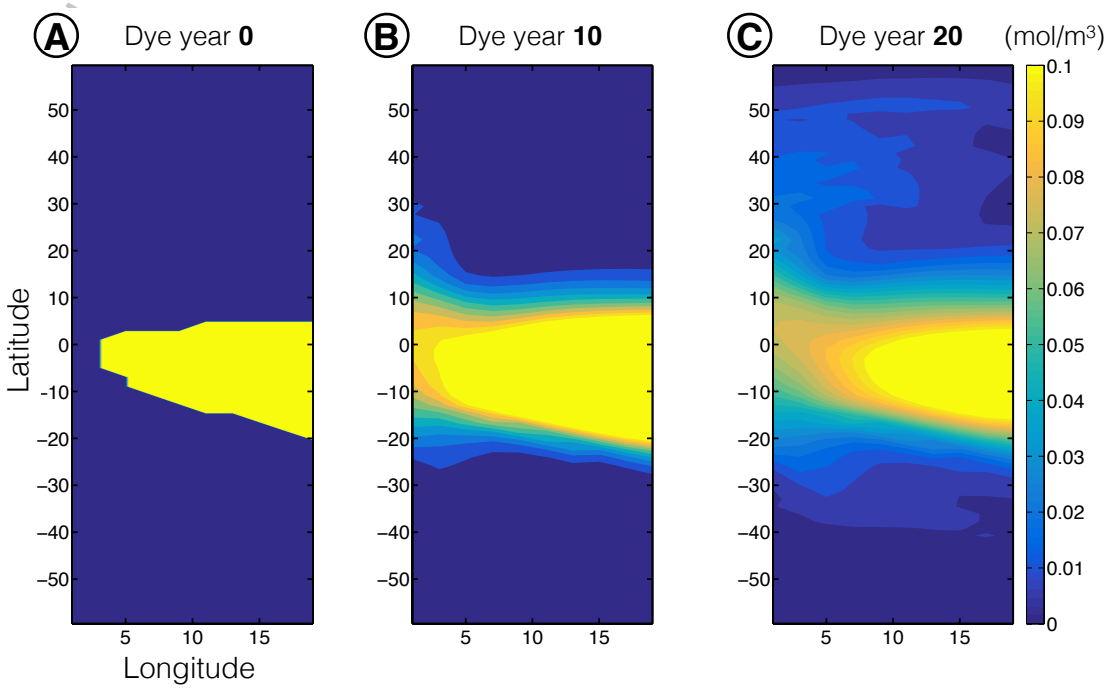

Figure 9. Passive dye tracer along the unperturbed $\sigma_\theta = 26$ kg/m^{3}surface after A) 0, B) 10 and C) 20 years in an unperturbed control simulation.

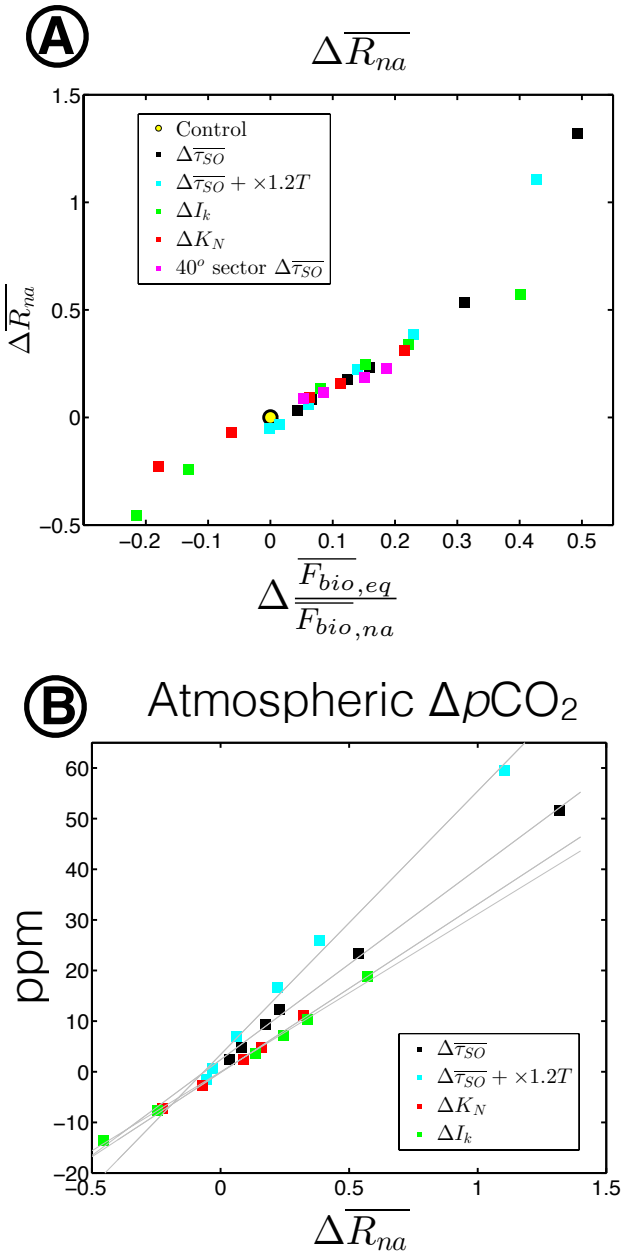

Figure 10. A) Change in $\overline{R_{na}}$ as function of $\frac{\overline{F_{bio,eq}}}{\overline{F_{bio,na}}}$ calculated from experiments with wind stress perturbations alone (black squares), wind stress alone in the 40° longitude model (magenta), wind stress and temperature perturbations (cyan squares), light half-saturation constant perturbations (green squares) and nutrient half-saturation constant perturbations (red squares). B) Change in pCO_2^a as a function of $\Delta\overline{R_{na}}$ (legend as in panel A).